Xiong and Li
EURASIP Journal on Advances in Signal Processing (2024) 2024:52
https://doi.org/10.1186/s13634-024-01151-1

EURASIP Journal on Advances in Signal Processing

RESEARCH Open Access

Temporally-correlated massive access: joint user activity detection and channel estimation via vector approximate message passing

Yueyue Xiong[1*] and Wei Li[1]

*Correspondence: 27894638@qq.com

[1] Zhongzi Huake Transportation Construction Technology Co., Ltd, Beijing 100195, China

Abstract

In the paper, we investigate a massive machine-type communication (mMTC), where numerous single-antenna users communicate with a single-antenna base station while being active. However, the status of user can undergoes multiple transitions between active and inactive states across whole consecutive intervals. Then, we formulate the problem of joint user activity detection and channel estimation within the dynamic compressed sensing (DCS) framework, considering the temporally-correlated user activity across the entire consecutive intervals. To be specific, we introduce a new hybrid vector approximate message passing algorithm for DCS (HyVAMP-DCS). The proposed algorithm comprises a VAMP block for estimating channel and a loopy belief propagation (LBP) block for detecting user activity. Moreover, these two blocks can exchange messages, enhancing the performance of both channel estimation and user activity detection. Importantly, compared to the fragile GAMP algorithm, VAMP is robust and applicable to a much broader class of large random matrices. Furthermore, the fixed points of VAMP's state evolution align with the replica prediction of the minimum mean-squared error. The simulation results illustrate the superiority of HyVAMP-DCS, demonstrating its significant outperformance over HyGAMP-DCS.

Keywords: Temporally-correlated user activity, User activity detection, Channel estimation, Dynamic compressed sensing, Hybrid vector approximate message passing

1 Introduction

In the paper, we investigate the problem of joint user activity detection and channel estimation within the massive machine-type communications (mMTC) scenario. As a key technology in 5G mobile communication networks, mMTC enables wireless connectivity among a massive number of devices in various applications, such as smart cities, monitoring, asset tracking, the Internet of Things (IoT), semantic communication [1, 2], and others [3, 4]. Compared to traditional human-centric communications, mMTC's traffic features include massive user devices, sporadic user activity, and short data packets [5]. In the context of mMTC, the grant-free access protocol has been regarded as a feasible approach, facilitating access for massive user devices [6, 7]. The protocol pre-allocates a unique pilot sequence to each device for identification and

channel estimation. In general, massive user devices primarily remain in a sleep state for energy efficiency. When a device is activated by external events, it will transmit its own sequence directly to the base station without requiring permission. Subsequently, the base station receives the observed signal, which is then utilized to jointly detect user activity and estimate channel.

Typically, in addressing the problem of joint user activity detection and channel estimation, characterized as a high-dimensional sparse signal recovery, various compressed sensing methods have been proposed, such as the neural network method [8], the sparsity-constrained method [9], the standard compressed sensing algorithm of orthogonal matching pursuit and basis pursuit denoising [10], the variants of approximate message passing (AMP) algorithm [6, 7, 11–13], and the variants of vector approximate message passing (VAMP) algorithm [14], and others. But these above algorithms have a limitation, i.e., they assume that all user devices maintain an active or inactive state throughout the entire consecutive intervals for jointly detecting user activity and estimating channel.

Indeed, in various practical applications of mMTC, devices cannot maintain a single state consistently throughout the entire consecutive intervals, i.e., their state undergoes multiple transitions between active and inactive states across whole consecutive intervals. Such situation means that the device activities are temporally-correlated. Therefore, to fully exploit the temporally-correlated user activity, [15–17] reformulate the problem of joint user activity detection and channel estimation of interest as dynamic compressed sensing (DCS), taking into account both sporadic user activity and the temporal correlation of user activities. For such DCS problem, various high-dimensional sparse signal recovery methods have been proposed, such as the convex relaxation methods [15, 18], the Bayesian framework [16, 19], the methods based on message passing [20, 21], and others. Specifically, [20] establishes a probabilistic model to depict the temporal correlation of user activity, provides the associated message passing schedule for executing the message passing algorithm [22], and introduces a novel sequential message passing algorithm for the recursive recovery of the target signal. [23] introduces the HyGAMP-DCS algorithm, aiming to fully leverage temporally-correlated user activities across the whole consecutive intervals. This algorithm integrates the computationally efficient GAMP algorithm [24–26] for channel estimation and the standard message passing algorithm [22] for updating user activity. However, the GAMP algorithm is fragile, as even small deviations from the i.i.d. sub-Gaussian model can cause the algorithm to diverge [27, 28]. Conversely, the VAMP algorithm is robust and holds under a much broader class of large random matrices $\boldsymbol{H}$. Additionally, the fixed points of VAMP's state evolution align with the replica prediction of the minimum mean-squared error [27, 28]. The HyVAMP-DCS's complexity order is dominated by matrix inversion per iteration [in Line 5 and 30]. However, after performing an initial singular value decomposition (SVD), HyVAMP-DCS has similar complexity to HyGAMP-DCS but is much more robust with respect to matrix $\boldsymbol{H}$ [27, 28].

In this work, inspired from [14, 29], we investigate the DCS problem of joint user activity detection and channel estimation across consecutive intervals, taking the temporal correlation of user activity and the correlated pilot cases into account.

The main contributions of this work are summarized as follows:

- The paper proposes to address the DCS problem of joint user activity detection and channel estimation across consecutive intervals, considering the temporal correlation of user activity;
- Unlike [20, 21], based on GAMP [24–26], this paper introduces the hybrid VAMP algorithm for the above DCS problem, abbreviated as HyVAMP-DCS. The proposed algorithm utilizes the computationally efficient VAMP algorithm [27, 28, 30, 31], which is suitable for correlated cases, for channel estimation. Additionally, it employs the loopy belief propagation (LBP) [32] for detecting user activities. The numerical results demonstrate the superiority of HyVAMP-DCS.

Notation: Throughout this document, we adopt the following notation conventions: Non-bold lowercase letters (e.g., m and ν) represent scalars, bold lowercase letters (e.g., $\boldsymbol{m}$ and $\boldsymbol{\nu}$) denote column vectors, and capital letters (e.g., $\boldsymbol{V}$ and $\boldsymbol{C}$) signify matrices. $\delta(\cdot)$ denotes a Dirac delta function. $\mathsf{N}[\boldsymbol{m}, \boldsymbol{C}]$ denotes a Gaussian distribution with mean $\boldsymbol{m}$ and covariance $\boldsymbol{C}$, defined as $\mathsf{N}[\boldsymbol{x}|\boldsymbol{m}, \boldsymbol{C}] \triangleq |2\pi \boldsymbol{C}|^{-\frac{1}{2}} \mathsf{e}[-\frac{1}{2}(\boldsymbol{x}-\boldsymbol{m})^{\mathsf{T}}\boldsymbol{C}^{-1}(\boldsymbol{x}-\boldsymbol{m})]$. For any matrix $\boldsymbol{A}$, $a_{i,j}$ represents the element at the i-th row and j-th column of $\boldsymbol{A}$. $\boldsymbol{A}^{\mathsf{T}}$ denotes the transpose of matrix $\boldsymbol{A}$. $\mathsf{D}(\boldsymbol{\nu})$ is a diagonal matrix with diagonal elements equal to the elements of vector $\boldsymbol{\nu}$. $\mathsf{d}(\boldsymbol{C})$ is a diagonal operator, returning a N-dimensional column vector containing the diagonal elements of matrix $\boldsymbol{C}$. $\mathbf{1}_N$ is a column vector of size N consisting of all ones. $\odot$ and $\oslash$ denote element-wise vector multiplication and division, respectively.

2 System model

In the work, we investigate the uplink of a mMTC scenario, consisting of a single base station and N devices, where they both equip with a single antenna. The observed signal $\boldsymbol{Y} \in \mathbb{C}^{M\times K}$ at base station can be modeled as:

$$\boldsymbol{Y} \sim p(\boldsymbol{Y}|\boldsymbol{Z}) \triangleq \prod_{i=1}^{M}\prod_{j=1}^{K} p(y_{i,j}|z_{i,j}), \quad \boldsymbol{Z} \triangleq \boldsymbol{H}\boldsymbol{X}, \tag{1}$$

where $\boldsymbol{H} \in \mathbb{C}^{M\times N}$ is the determined pilot matrix and $\boldsymbol{X} \in \mathbb{C}^{N\times K}$ is the composite channel matrix to be estimated. Firstly, we characterize $x_{n,k}$ as a composition of channel and the user activity $a_{n,k}$, which can be described by a Bernoulli–Gaussian distribution as:

$$p(x_{n,k}|a_{n,k}) \triangleq (1-a_{n,k})\delta(x_{n,k}) + a_{n,k}\mathsf{N}[x_{n,k}|0, \nu_{\mathsf{x}}], \tag{2}$$

where $a_{n,k} \in \{0, 1\}$ indicates the status for user n at the k-th interval. Next, we model the transition of temporally-correlated user activities for user n across entire consecutive intervals as a Markov chain. Then, assuming that the activation probability of user n at the k-th interval is p_{a}, the transition probability matrix of the Markov chain is expressed as:

$$\boldsymbol{B} \triangleq \begin{bmatrix} b_{00} & b_{01} \\ b_{10} & b_{11} \end{bmatrix},$$

where $b_{10} \triangleq p(a_{n,k}=0|a_{n,k-1}=1)$ and other three similar transition probabilities are denoted as: $b_{01}=p_{\mathsf{a}}b_{10}/(1-p_{\mathsf{a}})$, $b_{00}=1-b_{01}$, and $b_{11}=1-b_{10}$. Finally, we represent the aforementioned Markov chain as a probability form as:

$$p(a_{n,1}|a_{n,0}) \triangleq (1-p_{\mathsf{a}})(1-a_{n,1})+p_{\mathsf{a}}a_{n,1}, \tag{3}$$

$$\begin{aligned} p(a_{n,k}|a_{n,k-1}) \triangleq & (1-a_{n,k-1})a_{n,k}b_{01}+a_{n,k-1}(1-a_{n,k})b_{10}+ \\ & (1-a_{n,k-1})(1-a_{n,k})b_{00}+a_{n,k-1}a_{n,k}b_{11}. \end{aligned} \tag{4}$$

3 The HyVAMP-DCS algorithm

In this paper, our goal is to jointly detect the temporally-correlated user activities $\boldsymbol{A}$ and estimate the composite channels $\boldsymbol{X}$ from the observed signal $\boldsymbol{Y}$ with the determined pilot matrix $\boldsymbol{H}$. We introduce the HyVAMP-DCS algorithm, which incorporates the VAMP [26, 28, 33] block for channel estimation and the LBP block for user activity detection.

By combining (2)–(4), the joint probability of system model (1) is expressed as:

$$p(\boldsymbol{Y},\boldsymbol{Z},\boldsymbol{X},\boldsymbol{A}) \triangleq \prod_{k=1}^{K}\left[p(\boldsymbol{y}_k|\boldsymbol{z}_k)\delta(\boldsymbol{z}_k-\boldsymbol{H}\boldsymbol{x}_k)\prod_{n=1}^{N}p(x_{n,k}|a_{n,k})p(a_{n,k}|a_{n,k-1})\right]. \tag{5}$$

Then, following the Bayes' rule, we can calculate the posterior probability of $\boldsymbol{Z}$, $\boldsymbol{X}$, and $\boldsymbol{A}$ as:

$$\begin{aligned} p(\boldsymbol{Z},\boldsymbol{X},\boldsymbol{A}|\boldsymbol{Y}) &\triangleq \frac{1}{p(\boldsymbol{Y})}p(\boldsymbol{Y},\boldsymbol{Z},\boldsymbol{X},\boldsymbol{A}), \\ p(\boldsymbol{Y}) &\triangleq \int \mathrm{d}\boldsymbol{Z}\mathrm{d}\boldsymbol{X}\mathrm{d}\boldsymbol{A}\, p(\boldsymbol{Y},\boldsymbol{Z},\boldsymbol{X},\boldsymbol{A}). \end{aligned} \tag{6}$$

In the Bayesian inference framework, we compute the minimum mean square error (MMSE) estimators for $x_{n,k}$ and $a_{n,k}$ based on the principle of MMSE, i.e.,

$$\hat{x}_{n,k} \triangleq \int \mathrm{d}x_{n,k}\, x_{n,k}p(x_{n,k}|\boldsymbol{Y}), \tag{7}$$

$$\hat{a}_{n,k} \triangleq \int \mathrm{d}a_{n,k}\, a_{n,k}p(a_{n,k}|\boldsymbol{Y}), \tag{8}$$

with

$$p(x_{n,k}|\boldsymbol{Y}) \triangleq \int \mathrm{d}\boldsymbol{Z}\mathrm{d}\boldsymbol{X}_{\setminus n,k}\mathrm{d}\boldsymbol{A}\, p(\boldsymbol{Z},\boldsymbol{X},\boldsymbol{A}|\boldsymbol{Y}), \tag{9}$$

$$p(a_{n,k}|\boldsymbol{Y}) \triangleq \int \mathrm{d}\boldsymbol{Z}\mathrm{d}\boldsymbol{X}\mathrm{d}\boldsymbol{A}_{\setminus n,k}\, p(\boldsymbol{Z},\boldsymbol{X},\boldsymbol{A}|\boldsymbol{Y}). \tag{10}$$

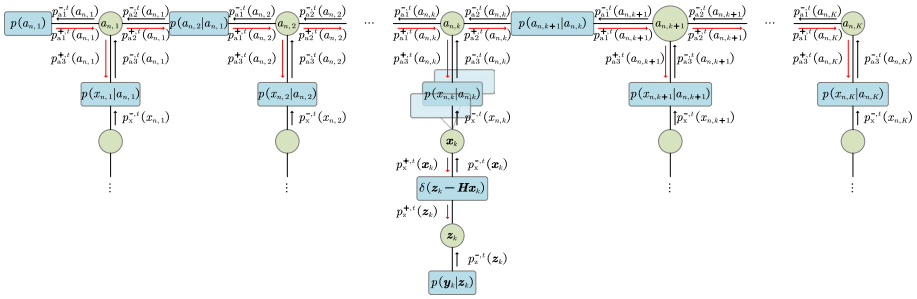

Fig. 1 The factor graph representation of the joint distribution (5)

Table 1 Message definitions in the factor graph

$p_{\mathsf{a1}}^{-,t}(a_{n,1})$	Message from $a_{n,1}$ to $p(a_{n,1})$
$p_{\mathsf{a1}}^{+,t}(a_{n,1})$	Message from $p(a_{n,1})$ to $a_{n,1}$
$p_{\mathsf{a1}}^{-,t}(a_{n,k})$	Message from $a_{n,k}$ to $p(a_{n,k}\|a_{n,k-1}), k \geq 2$
$p_{\mathsf{a1}}^{+,t}(a_{n,k})$	Message from $p(a_{n,k}\|a_{n,k-1})$ to $a_{n,k}, k \geq 2$
$p_{\mathsf{a2}}^{-,t}(a_{n,k})$	Message from $p(a_{n,k+1}\|a_{n,k})$ to $a_{n,k}, k \leq K-1$
$p_{\mathsf{a2}}^{+,t}(a_{n,k})$	Message from $a_{n,k}$ to $p(a_{n,k+1}\|a_{n,k}), k \leq K-1$
$p_{\mathsf{a3}}^{-,t}(a_{n,k})$	Message from $p(x_{n,k}\|a_{n,k})$ to $a_{n,k}$
$p_{\mathsf{a3}}^{+,t}(a_{n,k})$	Message from $a_{n,k}$ to $p(x_{n,k}\|a_{n,k})$
$p_{\mathsf{x}}^{-,t}(\boldsymbol{x}_k)$	Message from $\delta(\boldsymbol{z}_k - \boldsymbol{H}\boldsymbol{x}_k)$ to $\boldsymbol{x}_k$
$p_{\mathsf{x}}^{+,t}(\boldsymbol{x}_k)$	Message from $\boldsymbol{x}_k$ to $\delta(\boldsymbol{z}_k - \boldsymbol{H}\boldsymbol{x}_k)$
$p_{\mathsf{z}}^{-,t}(\boldsymbol{z}_k)$	Message from $p(\boldsymbol{y}_k\|\boldsymbol{z}_k)$ to $\boldsymbol{z}_k$
$p_{\mathsf{z}}^{+,t}(\boldsymbol{z}_k)$	Message from $\delta(\boldsymbol{z}_k - \boldsymbol{H}\boldsymbol{x}_k)$ to $\boldsymbol{z}_k$

Although directly computing high-dimensional integral in (9)–(10) is intractable, variants of message passing can empirically approximate these.

Following the approach of hybrid decentralized generalized expectation consistent (HyDeGEC) [14], we introduce the HyVAMP-DCS algorithm for our interested DCS problem, involving joint temporally-correlated user activity detection and channel estimation. The HyVAMP-DCS algorithm consists of VAMP block for channel estimation and LBP block for temporally-correlated user activity detection. Throughout the iterative process, the two blocks exchange messages, leading to a significant enhancement in both channel estimation and user detection performance. We introduce the details of the HyVAMP-DCS algorithm in the following literature. Firstly, a factor graph is proposed to illustrate the joint probability (5), as depicted in Fig. 1. Then, we define all messages in the factor graph, as described in Tab. 1.

3.1 VAMP block for channel estimation

In the part, we introduce the VAMP algorithm [27, 28] for channel estimation. Specifically, we provide an approximate derivation of (9). The VAMP block includes all messages of the area between variable nodes $\{\boldsymbol{x}_k\}$ and factor nodes $\{p(\boldsymbol{y}_k|\boldsymbol{z}_k)\}$. Then, the

basic VAMP algorithm is given in Lines 2-8 and 27-35 of Algo. 1. Specifically, to compute the MMSE estimator of $\boldsymbol{X}$, we substitute the message $p_{\mathsf{a3}}^{+,t}(a_{n,k})$ into $p(x_{n,k}|a_{n,k})$ to derive $p(x_{n,k})$:

$$\begin{aligned} p(x_{n,k}) &= \int \mathrm{d}a_{n,k}\, p(x_{n,k}|a_{n,k}) p_{\mathsf{a3}}^{+,t+1}(a_{n,k}) \\ &= (1-q_{\mathsf{a3},n,k}^{+,t+1})\delta(x_{n,k}) + q_{\mathsf{a3},n,k}^{+,t+1}\mathsf{N}[x_{n,k}|0,\nu_{\mathsf{x}}]. \end{aligned}$$

Then, we proceed to merge $p(x_{n,k})$ into $p_{\mathsf{x}}^{-,t}(x_{n,k})$ to produce the approximate posterior marginal distribution of $x_{n,k}$:

$$\begin{aligned} p(x_{n,k}|\boldsymbol{Y}) =& \frac{1}{C_{n,k}}\mathsf{N}[x_{n,k}|m_{\mathsf{x},n,k}^{-,t},\nu_{\mathsf{x},n,k}^{-,t}]p(x_{n,k}) \\ =& \frac{1}{C_{n,k}}\{(1-q_{\mathsf{a3},n,k}^{+,t+1})\mathsf{N}[m_{\mathsf{x},n,k}^{-,t}|0,\nu_{\mathsf{x},n,k}^{-,t}]\delta(x_{n,k}) \\ &+ q_{\mathsf{a3},n,k}^{+,t+1}\mathsf{N}[m_{\mathsf{x},n,k}^{-,t}|0,\nu_{\mathsf{x}}+\nu_{\mathsf{x},n,k}^{-,t}]\mathsf{N}[x_{n,k}|\hat{m}_{n,k},\hat{\nu}_{n,k}]\}, \\ C_{n,k} =& \int \mathrm{d}x_{n,k}\, \mathsf{N}[x_{n,k}|m_{\mathsf{x},n,k}^{-,t},\nu_{\mathsf{x},n,k}^{-,t}]p(x_{n,k}) \\ =& (1-q_{\mathsf{a3},n,k}^{+,t+1})\mathsf{N}[m_{\mathsf{x},n,k}^{-,t}|0,\nu_{\mathsf{x},n,k}^{-,t}] + q_{\mathsf{a3},n,k}^{+,t+1}\mathsf{N}[m_{\mathsf{x},n,k}^{-,t}|0,\nu_{\mathsf{x}}+\nu_{\mathsf{x},n,k}^{-,t}], \end{aligned}$$

with $\hat{\nu}_{n,k} \triangleq (\frac{1}{\nu_{\mathsf{x}}} + \frac{1}{\nu_{\mathsf{x},n,k}^{-,t}})^{-1}$ and $\hat{m}_{n,k} \triangleq \hat{\nu}_{n,k}\frac{m_{\mathsf{x},n,k}^{-,t}}{\nu_{\mathsf{x},n,k}^{-,t}}$. Finally, we can obtain explicit expression of the posterior mean and variance of $x_{n,k}$ in the Line 27 of Algo. 1 as:

$$\hat{m}_{\mathsf{x},n,k}^{+,t+1} = w_{n,k}\hat{m}_{n,k}, \tag{11}$$

$$\begin{aligned} \hat{\nu}_{\mathsf{x},n,k}^{+,t+1} =& w_{n,k}\hat{\nu}_{n,k} + (w_{n,k}-w_{n,k}^2)\hat{m}_{n,k}^2, \\ w_{n,k} \triangleq& \frac{1}{C_{n,k}} q_{\mathsf{a3},n,k}^{+,t+1}\mathsf{N}[m_{\mathsf{x},n,k}^{-,t}|0,\nu_{\mathsf{x}}+\nu_{\mathsf{x},n,k}^{-,t}]. \end{aligned} \tag{12}$$

Given that the LBP block updates $p_{\mathsf{a3}}^{+,t+1}(a_{n,k})$ at every iteration, Eqs. (11)–(12) can also be updated at each iteration.

3.2 LBP block for user activity detection

In the subsection, we introduce the LBP block [32] for user activity detection. The LBP block includes all messages of the area between factor nodes $\{p(a_{n,1})\}$ and factor nodes $\{p(x_{n,k}|a_{n,k})\}$. Moreover, we employ the LBP block to update the activity probability of each user using the message $p_{\mathsf{x}}^{-,t}(x_{n,k})$ received from the VAMP block. We now schedule the messages in the LBP block by the following manner:

- **Backward propagation:** For any interval, $p_{\mathsf{a3}}^{-,t}(a_{n,k})$ is denoted as:

$$p_{\mathsf{a3}}^{-,t}(a_{n,k}) = \int \mathrm{d}x_{n,k}\, p_{\mathsf{x}}^{-,t}(x_{n,k})p(x_{n,k}|a_{n,k}). \tag{13}$$

  For K-th interval, $p_{\mathsf{a1}}^{-,t}(a_{n,K})$ is represented as:

$$p_{\mathsf{a1}}^{-,t}(a_{n,K}) = p_{\mathsf{a3}}^{-,t}(a_{n,K}). \tag{14}$$

For k-th interval ($k = 1, \cdots, K-1$), $p_{\mathsf{a2}}^{-,t}(a_{n,k})$ and $p_{\mathsf{a1}}^{-,t}(a_{n,k})$ are sequentially computed as:

$$p_{\mathsf{a2}}^{-,t}(a_{n,k}) = \int \mathsf{d}a_{n,k+1}\, p_{\mathsf{a1}}^{-,t}(a_{n,k+1}) p(a_{n,k+1}|a_{n,k}), \tag{15}$$

$$p_{\mathsf{a1}}^{-,t}(a_{n,k}) = p_{\mathsf{a2}}^{-,t}(a_{n,k}) p_{\mathsf{a3}}^{-,t}(a_{n,k}); \tag{16}$$

- **Forward propagation:** For 1-st interval, $p_{\mathsf{a1}}^{+,t+1}(a_{n,1})$, $p_{\mathsf{a2}}^{+,t+1}(a_{n,1})$, and $p_{\mathsf{a3}}^{+,t+1}(a_{n,1})$ are sequentially calculated as:

$$p_{\mathsf{a1}}^{+,t+1}(a_{n,1}) = p(a_{n,1}), \tag{17}$$

$$p_{\mathsf{a2}}^{+,t+1}(a_{n,1}) = p_{\mathsf{a1}}^{+,t+1}(a_{n,1}) p_{\mathsf{a3}}^{-,t}(a_{n,1}), \tag{18}$$

$$p_{\mathsf{a3}}^{+,t+1}(a_{n,1}) = p_{\mathsf{a1}}^{+,t+1}(a_{n,1}) p_{\mathsf{a2}}^{-,t}(a_{n,1}). \tag{19}$$

For k-th interval ($k = 2, \cdots, K-1$), $p_{\mathsf{a1}}^{+,t+1}(a_{n,k})$, $p_{\mathsf{a2}}^{+,t+1}(a_{n,k})$, and $p_{\mathsf{a3}}^{+,t+1}(a_{n,k})$ are sequentially denoted as:

$$p_{\mathsf{a1}}^{+,t+1}(a_{n,k}) = \int \mathsf{d}a_{n,k-1}\, p(a_{n,k}|a_{n,k-1}) p_{\mathsf{a2}}^{+,t+1}(a_{n,k-1}), \tag{20}$$

$$p_{\mathsf{a2}}^{+,t+1}(a_{n,k}) = p_{\mathsf{a1}}^{+,t+1}(a_{n,k}) p_{\mathsf{a3}}^{-,t}(a_{n,k}), \tag{21}$$

$$p_{\mathsf{a3}}^{+,t+1}(a_{n,k}) = p_{\mathsf{a1}}^{+,t+1}(a_{n,k}) p_{\mathsf{a2}}^{-,t}(a_{n,k}). \tag{22}$$

For K-th interval, $p_{\mathsf{a1}}^{+,t+1}(a_{n,K})$ and $p_{\mathsf{a3}}^{+,t+1}(a_{n,K})$ are sequentially expressed as:

$$p_{\mathsf{a1}}^{+,t+1}(a_{n,K}) = \int \mathsf{d}a_{n,K-1}\, p(a_{n,K}|a_{n,K-1}) p_{\mathsf{a2}}^{+,t+1}(a_{n,K-1}), \tag{23}$$

$$p_{\mathsf{a3}}^{+,t+1}(a_{n,K}) = p_{\mathsf{a1}}^{+,t+1}(a_{n,K}). \tag{24}$$

Before the iteration, we initial all the messages as Bernoulli distribution.

For (13), we evaluate $p_{\mathsf{a3}}^{-,t}(a_{n,k})$ as:

$$\begin{aligned} p_{\mathsf{a3}}^{-,t}(a_{n,k}) &= \int \mathsf{d}x_{n,k}\, p_{\mathsf{x}}^{-,t}(x_{n,k}) p(x_{n,k}|a_{n,k}) \\ &= (1 - q_{\mathsf{a3},n,k}^{-,t})(1 - a_{n,k}) + q_{\mathsf{a3},n,k}^{-,t} a_{n,k}, \end{aligned}$$

with

$$q_{\mathsf{a3},n,k}^{-,t} \triangleq \frac{\mathsf{N}[m_{\mathsf{x},n,k}^{-,t}|0, \nu_{\mathsf{x}} + \nu_{\mathsf{x},n,k}^{-,t}]}{\mathsf{N}[m_{\mathsf{x},n,k}^{-,t}|0, \nu_{\mathsf{x},n,k}^{-,t}] + \mathsf{N}[m_{\mathsf{x},n,k}^{-,t}|0, \nu_{\mathsf{x}} + \nu_{\mathsf{x},n,k}^{-,t}]}.$$

For (14), we compute $p_{\mathsf{a1}}^{-,t}(a_{n,K})$ with $q_{\mathsf{a1},n,K}^{-,t} = q_{\mathsf{a3},n,K}^{-,t}$.

For (15), we represent $q_{\mathsf{a2},n,k}^{-,t}$ as:

$$\begin{aligned} p_{\mathsf{a2}}^{-,t}(a_{n,k}) &= \int \mathrm{d}a_{n,k+1}\, p_{\mathsf{a1}}^{-,t}(a_{n,k+1}) p(a_{n,k+1}|a_{n,k}) \\ &= (1 - q_{\mathsf{a2},n,k}^{-,t})(1 - a_{n,k}) + q_{\mathsf{a2},n,k}^{-,t} a_{n,k}, \end{aligned}$$

with

$$q_{\mathsf{a2},n,k}^{-,t} \triangleq \frac{b_{11} q_{\mathsf{a1},n,k+1}^{-,t} + b_{10}(1 - q_{\mathsf{a1},n,k+1}^{-,t})}{(b_{00} + b_{10})(1 - q_{\mathsf{a1},n,k+1}^{-,t}) + (b_{01} + b_{11}) q_{\mathsf{a1},n,k+1}^{-,t}}.$$

For (16), we evaluate $p_{\mathsf{a1}}^{-,t}(a_{n,k})$ as:

$$\begin{aligned} p_{\mathsf{a1}}^{-,t}(a_{n,k}) &= p_{\mathsf{a2}}^{-,t}(a_{n,k}) p_{\mathsf{a3}}^{-,t}(a_{n,k}) \\ &= (1 - q_{\mathsf{a1},n,k}^{-,t})(1 - a_{n,k}) + q_{\mathsf{a1},n,k}^{-,t} a_{n,k}, \end{aligned}$$

with

$$q_{\mathsf{a1},n,k}^{-,t} \triangleq \frac{q_{\mathsf{a2},n,k}^{-,t} q_{\mathsf{a3},n,k}^{-,t}}{(1 - q_{\mathsf{a2},n,k}^{-,t})(1 - q_{\mathsf{a3},n,k}^{-,t}) + q_{\mathsf{a2},n,k}^{-,t} q_{\mathsf{a3},n,k}^{-,t}}.$$

For (17), we denote $p_{\mathsf{a1}}^{+,t+1}(a_{n,1})$ with $q_{\mathsf{a1},n,1}^{+,t+1} = p_{\mathsf{a}}$.

For (18) and (21), we evaluate $p_{\mathsf{a2}}^{+,t+1}(a_{n,k})$ as:

$$\begin{aligned} p_{\mathsf{a2}}^{+,t+1}(a_{n,k}) &= p_{\mathsf{a1}}^{+,t+1}(a_{n,k}) p_{\mathsf{a3}}^{-,t}(a_{n,k}) \\ &= (1 - q_{\mathsf{a2},n,k}^{+,t+1})(1 - a_{n,k}) + q_{\mathsf{a2},n,k}^{+,t+1} a_{n,k}, \end{aligned}$$

with

$$q_{\mathsf{a2},n,k}^{+,t+1} \triangleq \frac{q_{\mathsf{a1},n,k}^{+,t+1} q_{\mathsf{a3},n,k}^{-,t}}{(1 - q_{\mathsf{a1},n,k}^{+,t+1})(1 - q_{\mathsf{a3},n,k}^{-,t}) + q_{\mathsf{a1},n,k}^{+,t+1} q_{\mathsf{a3},n,k}^{-,t}}.$$

For (19) and (22), we compute $p_{\mathsf{a3}}^{+,t+1}(a_{n,k})$ as:

$$\begin{aligned} p_{\mathsf{a3}}^{+,t+1}(a_{n,k}) &= p_{\mathsf{a1}}^{+,t+1}(a_{n,k}) p_{\mathsf{a2}}^{-,t}(a_{n,k}) \\ &= (1 - q_{\mathsf{a3},n,k}^{+,t+1})(1 - a_{n,k}) + q_{\mathsf{a3},n,k}^{+,t+1} a_{n,k}, \end{aligned}$$

with

$$q_{\mathsf{a3},n,k}^{+,t+1} \triangleq \frac{q_{\mathsf{a1},n,k}^{+,t+1} q_{\mathsf{a2},n,k}^{-,t}}{(1 - q_{\mathsf{a1},n,k}^{+,t+1})(1 - q_{\mathsf{a2},n,k}^{-,t}) + q_{\mathsf{a1},n,k}^{+,t+1} q_{\mathsf{a2},n,k}^{-,t}}.$$

For (20) and (23), we represent $p_{\mathsf{a1}}^{+,t+1}(a_{n,k})$ as:

$$\begin{aligned} p_{\mathsf{a1}}^{+,t+1}(a_{n,k}) =& \int \mathrm{d}a_{n,k-1}\, p(a_{n,k}|a_{n,k-1}) p_{\mathsf{a2}}^{+,t+1}(a_{n,k-1}) \\ =&(1-q_{\mathsf{a1},n,k}^{+,t+1})(1-a_{n,k}) + q_{\mathsf{a1},n,k}^{+,t+1} a_{n,k}, \end{aligned}$$

with

$$q_{\mathsf{a1},n,k}^{+,t+1} \triangleq b_{11} q_{\mathsf{a2},n,k-1}^{+,t+1} + b_{01}(1-q_{\mathsf{a2},n,k-1}^{+,t+1}).$$

For (24), we denote $p_{\mathsf{a3}}^{+,t+1}(a_{n,K})$ with $q_{\mathsf{a3},n,K}^{+,t+1} \triangleq q_{\mathsf{a1},n,K}^{+,t+1}$.

So far, we can summarize the HyVAMP-DCS algorithm as given in Algo. 1. For conciseness, we define several functions as following:

- **Extrinsic function:** $(\boldsymbol{m}_2, \boldsymbol{v}_2) \triangleq \mathsf{Ext}[\hat{\boldsymbol{m}}, \hat{\boldsymbol{v}}, \boldsymbol{m}_1, \boldsymbol{v}_1]$, with

$$\begin{aligned} \boldsymbol{v}_2 =& \mathbf{1} \oslash (\mathbf{1} \oslash \hat{\boldsymbol{v}} - \mathbf{1} \oslash \boldsymbol{v}_1), \\ \boldsymbol{m}_2 =& \boldsymbol{v}_2 \odot (\hat{\boldsymbol{m}} \oslash \hat{\boldsymbol{v}} - \boldsymbol{m}_1 \oslash \boldsymbol{v}_1); \end{aligned}$$

- **linear minimum mean square error (LMMSE) estimation:** $(\hat{\boldsymbol{m}}_{\mathsf{x}}, \hat{\boldsymbol{C}}_{\mathsf{x}}) \triangleq \mathbb{E}[\boldsymbol{m}_{\mathsf{x}}, \boldsymbol{v}_{\mathsf{x}}, \boldsymbol{m}_{\mathsf{z}}, \boldsymbol{v}_{\mathsf{z}}, \boldsymbol{H}]$, with

$$\begin{aligned} \hat{\boldsymbol{C}}_{\mathsf{x}} =& [\mathsf{D}(\mathbf{1} \oslash \boldsymbol{v}_{\mathsf{x}}) + \boldsymbol{H}^{\mathsf{H}} \mathsf{D}(\mathbf{1} \oslash \boldsymbol{v}_{\mathsf{z}}) \boldsymbol{H}]^{-1}, \\ \hat{\boldsymbol{m}}_{\mathsf{x}} =& \hat{\boldsymbol{C}}_{\mathsf{x}} [\boldsymbol{m}_{\mathsf{x}} \oslash \boldsymbol{v}_{\mathsf{x}} + \boldsymbol{H}^{\mathsf{H}} (\boldsymbol{m}_{\mathsf{z}} \oslash \boldsymbol{v}_{\mathsf{z}})]; \end{aligned}$$

- **Activity detection:** $\hat{\boldsymbol{A}} = \mathsf{Act}[\hat{\boldsymbol{Q}}] = \mathsf{sign}[\hat{\boldsymbol{Q}} \geq 0.5]$, where $\mathsf{sign}[\cdot]$ is a sign function.

4 Validation and discussion

To compare the performance of HyGAMP-DCS and HyVAMP-DCS (proposed), we carry out the Monte Carlo simulations and present the results below. We adopt a typical setting of $(M, N, K, T, \nu_{\mathsf{x}}, p_{\mathsf{a}}, b_{10}) = (200, 50, 300, 20, 0.02, 0.1, 0.6)$. Then, we apply an B-bit analog-to-digital converter (ADC) for $p(y|z)$, whose detailed formula could be found in [14, 28] among many others. The transitional density from z to y, denoted by $p(y|z)$, then particularizes into the following form

$$\begin{aligned} p(y|z) =& p(y_{\mathsf{R}}|z_{\mathsf{R}}) p(y_{\mathsf{I}}|z_{\mathsf{I}}), \\ p(y_{\mathsf{a}}|z_{\mathsf{a}}) =& \Phi[\frac{q^{\mathsf{h}}(y_{\mathsf{a}}) - z_{\mathsf{a}}}{\sigma}] - \Phi[\frac{q^{\mathsf{l}}(y_{\mathsf{a}}) - z_{\mathsf{a}}}{\sigma}]. \end{aligned}$$

where $\Phi(x)$ is the cumulative distribution function (CDF) of unit normal distribution. a_{R} and a_{I} denote the real and imaginary parts of the complex number a. $[q^{\mathsf{l}}(y_{\mathsf{a}}), q^{\mathsf{h}}(y_{\mathsf{a}})]$ defines the input interval for an output y_{a}. Then, we define the signal-to-noise ratio (SNR) as σ^{-2}.

To better simulate the impact of channel correlation, we assume a Kronecker model for the generation of correlated pilot matrix, i.e., $\boldsymbol{H} = \boldsymbol{H}_{\mathsf{w}} \boldsymbol{R}^{\frac{1}{2}}$, where $\boldsymbol{R}$ is a correlation matrix with $R_{i,j} \triangleq \rho^{|i-j|}$, for $i, j = 1, \cdots, N$ and $\rho \in [0, 1)$ is the correlated coefficient of the pilot matrix, and $\boldsymbol{H}_{\mathsf{w}}$ is taken from the constellation of 4-QAM. For correlated case of the pilot matrix $\boldsymbol{H}$, we use $\rho = 0.6$, while in the i.i.d. case, $\rho = 0$.

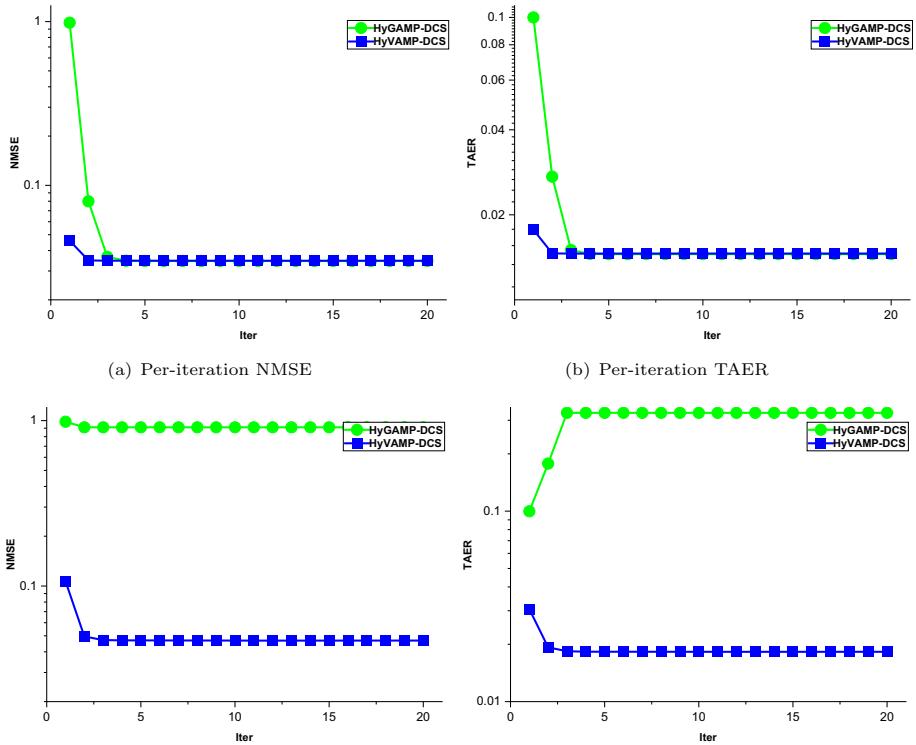

(a) Per-iteration NMSE (b) Per-iteration TAER

(c) Per-iteration NMSE (d) Per-iteration TAER

Fig. 2 Per-iteration NMSE and TAER for HyGAMP-DCS and HyVAMP-DCS. **a**, **b**: i.i.d. case, **c**, **d**: Correlated case

In all experiments, the performance metric used for user activity detection is defined as the time-averaged activity error ratio (TAER), denoted as

$$\mathsf{TAER} \triangleq \frac{\sum_{n=1}^{N}\sum_{k=1}^{K}|\hat{m}_{\mathsf{a},n,k}^{+,T+1} - a_{n,k}|}{NK}.$$

Furthermore, we utilize the normalized mean square error (NMSE) as the performance metric of channel estimation, expressed as:

$$\mathsf{NMSE} \triangleq \mathbb{E}[\frac{\|\hat{\boldsymbol{M}}_{\mathsf{x}}^{+,T+1} - \boldsymbol{X}\|_{\mathsf{F}}^2}{\|\boldsymbol{X}\|_{\mathsf{F}}^2}],$$

where $\|\boldsymbol{A}\|_{\mathsf{F}}$ denote the Frobenius norm of $\boldsymbol{A}$. Then, we have these remarks:

- **Per-iteration behavior of HyVAMP-DCS:** Given $B = 5$ and $\mathsf{SNR} = 10$, we compare the MSE performance of HyVAMP-DCS with HyGAMP-DCS. As shown in Fig. 2, the HyVAMP-DCS proposed is extremely effective: For the i.i.d. case, HyVAMP-DCS converges in only a few iterations, which is much faster than HyGAMP-DCS; for the correlated case, HyVAMP-DCS outperforms HyGAMP-DCS significantly.

Algorithm 1 HyVAMP-DCS

Require: $\boldsymbol{y}$, $\boldsymbol{A}$, $\{p(x_{n,k}|a_{n,k})\}$, $\{p(a_{n,k}|a_{n,k-1})\}$, $\forall n,k$
Ensure: $\boldsymbol{M}_{\mathsf{z}}^{+,1}$, $\boldsymbol{V}_{\mathsf{z}}^{+,1}$, $\boldsymbol{M}_{\mathsf{x}}^{+,1}$, $\boldsymbol{V}_{\mathsf{x}}^{+,1}$

while $t = 1, \cdots, T$ **do**
  $(\hat{\boldsymbol{M}}_{\mathsf{z}}^{-,t}, \hat{\boldsymbol{V}}_{\mathsf{z}}^{-,t}) = \mathbb{E}[\boldsymbol{Z}|\boldsymbol{M}_{\mathsf{z}}^{+,t}, \boldsymbol{V}_{\mathsf{z}}^{+,t}]$
  $(\boldsymbol{M}_{\mathsf{z}}^{-,t}, \boldsymbol{V}_{\mathsf{z}}^{-,t}) = \mathsf{Ext}[\hat{\boldsymbol{M}}_{\mathsf{z}}^{-,t}, \hat{\boldsymbol{V}}_{\mathsf{z}}^{-,t}, \boldsymbol{M}_{\mathsf{z}}^{+,t}, \boldsymbol{V}_{\mathsf{z}}^{+,t}]$
  while $k = 1, \cdots, K$ **do**
    $(\hat{\boldsymbol{m}}_{\mathsf{x},k}^{-,t}, \hat{\boldsymbol{C}}_{\mathsf{x},k}^{-,t}) = \mathbb{E}[\boldsymbol{m}_{\mathsf{x},k}^{+,t}, \boldsymbol{v}_{\mathsf{x},k}^{+,t}, \boldsymbol{m}_{\mathsf{z},k}^{-,t}, \boldsymbol{v}_{\mathsf{z},k}^{-,t}, \boldsymbol{H}]$
    $\hat{\boldsymbol{v}}_{\mathsf{x},k}^{-,t} = \mathsf{d}(\hat{\boldsymbol{C}}_{\mathsf{x},k}^{-,t})$
  end while
  $(\boldsymbol{M}_{\mathsf{x}}^{-,t}, \boldsymbol{V}_{\mathsf{x}}^{-,t}) = \mathsf{Ext}[\hat{\boldsymbol{M}}_{\mathsf{x}}^{-,t}, \hat{\boldsymbol{V}}_{\mathsf{x}}^{-,t}, \boldsymbol{M}_{\mathsf{x}}^{+,t}, \boldsymbol{V}_{\mathsf{x}}^{+,t}]$
  $\boldsymbol{Q}_{\mathsf{a3}}^{-,t} = \frac{\mathsf{N}[\boldsymbol{M}_{\mathsf{x}}^{-,t}|0, v_{\mathsf{x}}+\boldsymbol{V}_{\mathsf{x}}^{-,t}]}{\mathsf{N}[\boldsymbol{M}_{\mathsf{x}}^{-,t}|0, \boldsymbol{V}_{\mathsf{x}}^{-,t}]+\mathsf{N}[\boldsymbol{M}_{\mathsf{x}}^{-,t}|, v_{\mathsf{x}}+\boldsymbol{V}_{\mathsf{x}}^{-,t}]}$
  $\boldsymbol{q}_{\mathsf{a1},K}^{-,t} = \boldsymbol{q}_{\mathsf{a3},K}^{-,t}$
  while $k = K-1, \cdots, 1$ **do**
    $\boldsymbol{q}_{\mathsf{a2},k}^{-,t} = \frac{b_{11}\boldsymbol{q}_{\mathsf{a1},k+1}^{-,t}+b_{10}(1-\boldsymbol{q}_{\mathsf{a1},k+1}^{-,t})}{(b_{00}+b_{10})(1-\boldsymbol{q}_{\mathsf{a1},k+1}^{-,t})+(b_{01}+b_{11})\boldsymbol{q}_{\mathsf{a1},k+1}^{-,t}}$
    $\boldsymbol{q}_{\mathsf{a1},k}^{-,t} = \frac{\boldsymbol{q}_{\mathsf{a2},k}^{-,t}\boldsymbol{q}_{\mathsf{a3},k}^{-,t}}{(1-\boldsymbol{q}_{\mathsf{a2},k}^{-,t})(1-\boldsymbol{q}_{\mathsf{a3},k}^{-,t})+\boldsymbol{q}_{\mathsf{a2},k}^{-,t}\boldsymbol{q}_{\mathsf{a3},k}^{-,t}}$
  end while
  $\boldsymbol{q}_{\mathsf{a1},1}^{+,t+1} = p_{\mathsf{a}}$
  $\boldsymbol{q}_{\mathsf{a2},1}^{+,t+1} = \frac{\boldsymbol{q}_{\mathsf{a1},1}^{+,t+1}\boldsymbol{q}_{\mathsf{a3},1}^{-,t}}{(1-\boldsymbol{q}_{\mathsf{a1},1}^{+,t+1})(1-\boldsymbol{q}_{\mathsf{a3},1}^{-,t})+\boldsymbol{q}_{\mathsf{a1},1}^{+,t+1}\boldsymbol{q}_{\mathsf{a3},1}^{-,t}}$
  $\boldsymbol{q}_{\mathsf{a3},1}^{+,t+1} = \frac{\boldsymbol{q}_{\mathsf{a1},1}^{+,t+1}\boldsymbol{q}_{\mathsf{a2},1}^{-,t}}{(1-\boldsymbol{q}_{\mathsf{a1},1}^{+,t+1})(1-\boldsymbol{q}_{\mathsf{a2},1}^{-,t})+\boldsymbol{q}_{\mathsf{a1},1}^{+,t+1}\boldsymbol{q}_{\mathsf{a2},1}^{-,t}}$
  while $k = 2, \cdots, K-1$ **do**
    $\boldsymbol{q}_{\mathsf{a1},k}^{+,t+1} = b_{11}\boldsymbol{q}_{\mathsf{a2},k-1}^{+,t+1} + b_{01}(1-\boldsymbol{q}_{\mathsf{a2},k-1}^{+,t+1})$
    $\boldsymbol{q}_{\mathsf{a2},k}^{+,t+1} = \frac{\boldsymbol{q}_{\mathsf{a1},k}^{+,t+1}\boldsymbol{q}_{\mathsf{a3},k}^{-,t}}{(1-\boldsymbol{q}_{\mathsf{a1},k}^{+,t+1})(1-\boldsymbol{q}_{\mathsf{a3},k}^{-,t})+\boldsymbol{q}_{\mathsf{a1},k}^{+,t+1}\boldsymbol{q}_{\mathsf{a3},k}^{-,t}}$
    $\boldsymbol{q}_{\mathsf{a3},k}^{+,t+1} = \frac{\boldsymbol{q}_{\mathsf{a1},k}^{+,t+1}\boldsymbol{q}_{\mathsf{a2},k}^{-,t}}{(1-\boldsymbol{q}_{\mathsf{a1},k}^{+,t+1})(1-\boldsymbol{q}_{\mathsf{a2},k}^{-,t})+\boldsymbol{q}_{\mathsf{a1},k}^{+,t+1}\boldsymbol{q}_{\mathsf{a2},k}^{-,t}}$
  end while
  $\boldsymbol{q}_{\mathsf{a1},K}^{+,t+1} = b_{11}\boldsymbol{q}_{\mathsf{a2},K-1}^{+,t+1} + b_{01}(1-\boldsymbol{q}_{\mathsf{a2},K-1}^{+,t+1})$
  $\boldsymbol{q}_{\mathsf{a3},K}^{+,t+1} = \boldsymbol{q}_{\mathsf{a1},K}^{+,t+1}$
  $\hat{\boldsymbol{Q}}_{\mathsf{a}}^{+,t+1} = \frac{\boldsymbol{Q}_{\mathsf{a3}}^{+,t+1}\boldsymbol{Q}_{\mathsf{a3}}^{-,t}}{(1-\boldsymbol{Q}_{\mathsf{a3}}^{+,t+1})(1-\boldsymbol{Q}_{\mathsf{a3}}^{-,t})+\boldsymbol{Q}_{\mathsf{a3}}^{+,t+1}\boldsymbol{Q}_{\mathsf{a3}}^{-,t}}$
  $\hat{\boldsymbol{M}}_{\mathsf{a}}^{+,t+1} = \mathsf{Act}[\hat{\boldsymbol{Q}}_{\mathsf{a}}^{+,t+1}]$
  $(\hat{\boldsymbol{M}}_{\mathsf{x}}^{+,t+1}, \hat{\boldsymbol{V}}_{\mathsf{x}}^{+,t+1}) = \mathbb{E}[\boldsymbol{X}|\boldsymbol{M}_{\mathsf{x}}^{-,t}, \boldsymbol{V}_{\mathsf{x}}^{-,t}, \boldsymbol{Q}_{\mathsf{a3}}^{+,t+1}]$
  $(\boldsymbol{M}_{\mathsf{x}}^{+,t+1}, \boldsymbol{V}_{\mathsf{x}}^{+,t+1}) = \mathsf{Ext}[\hat{\boldsymbol{M}}_{\mathsf{x}}^{+,t+1}, \hat{\boldsymbol{V}}_{\mathsf{x}}^{+,t+1}, \boldsymbol{M}_{\mathsf{x}}^{-,t}, \boldsymbol{V}_{\mathsf{x}}^{-,t}]$
  while $k = 1, \cdots, K$ **do**
    $(\hat{\boldsymbol{m}}_{\tilde{\mathsf{x}},k}^{+,t+1}\hat{\boldsymbol{C}}_{\tilde{\mathsf{x}},k}^{+,t+1}) = \mathbb{E}[\boldsymbol{m}_{\mathsf{x},k}^{+,t+1}, \boldsymbol{v}_{\mathsf{x},k}^{+,t+1}, \boldsymbol{m}_{\mathsf{z},k}^{-,t}, \boldsymbol{v}_{\mathsf{z},k}^{-,t}, \boldsymbol{H}]$
    $\hat{\boldsymbol{m}}_{\mathsf{z},k}^{+,t+1} = \boldsymbol{H}\hat{\boldsymbol{m}}_{\tilde{\mathsf{x}},k}^{+,t+1}$
    $\hat{\boldsymbol{C}}_{\mathsf{z},k}^{+,t+1} = \boldsymbol{H}\hat{\boldsymbol{C}}_{\tilde{\mathsf{x}},k}^{+,t+1}\boldsymbol{H}^{\mathsf{H}}$
    $\hat{\boldsymbol{v}}_{\mathsf{z},k}^{+,t+1} = \mathsf{d}(\hat{\boldsymbol{C}}_{\mathsf{z},k}^{+,t+1})$
  end while
  $(\boldsymbol{M}_{\mathsf{z}}^{+,t+1}, \boldsymbol{V}_{\mathsf{z}}^{+,t+1}) = \mathsf{Ext}[\hat{\boldsymbol{M}}_{\mathsf{z}}^{+,t+1}, \hat{\boldsymbol{V}}_{\mathsf{z}}^{+,t+1}, \boldsymbol{M}_{\mathsf{z}}^{-,t}, \boldsymbol{V}_{\mathsf{z}}^{-,t}]$
end while

- **Robustness to parameter change:** We keep the above setting and vary the parameters of ρ, SNR, and B, alternatively. Fig. 3 and 4 show that HyVAMP-DCS is robust to such parameter change.

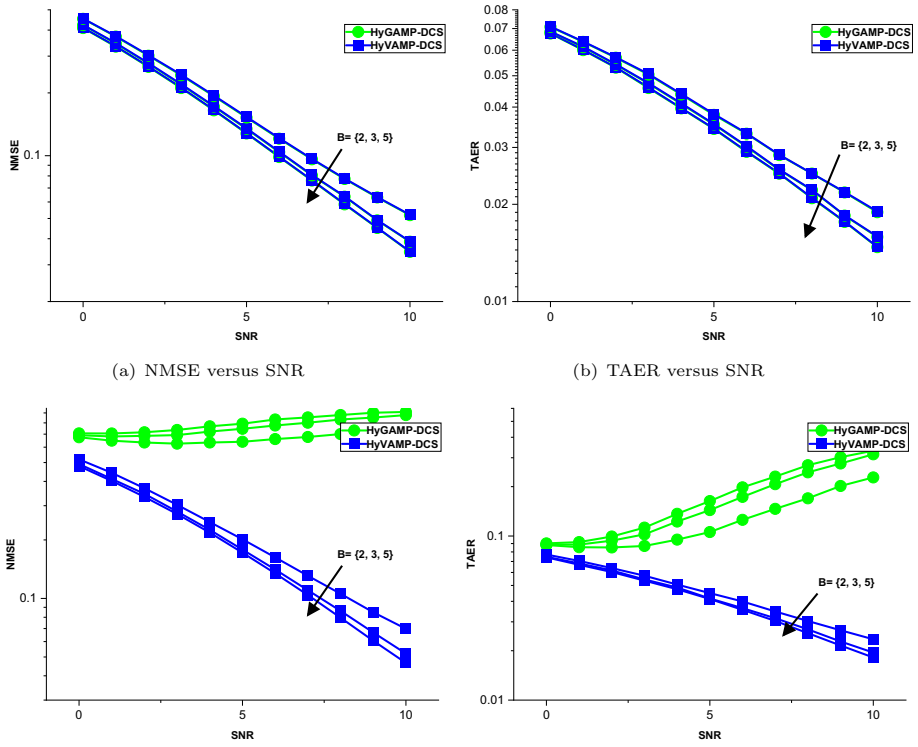

(a) NMSE versus SNR (b) TAER versus SNR

(c) NMSE versus SNR (d) TAER versus SNR

Fig. 3 NMSE and TAER versus SNR for HyGAMP-DCS and HyVAMP-DCS. **a**, **b**: i.i.d. case, **c**, **d**: Correlated case

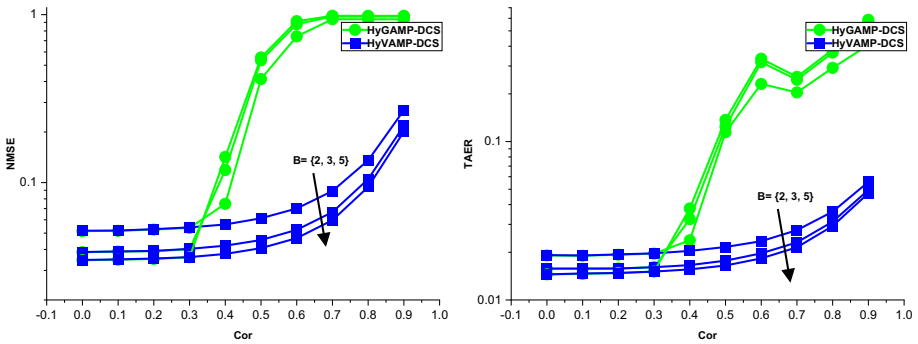

(a) NMSE versus ρ (b) TAER versus ρ

Fig. 4 NMSE and TAER versus ρ for HyGAMP-DCS and HyVAMP-DCS

5 Conclusion

In this work, we investigate the DCS problem of joint user activity detection and channel estimation within the mMTC scenario, considering the device activities are temporally-correlated across the entire consecutive intervals. Then, we present the HyVAMP-DCS algorithm, comprising a VAMP block for channel estimation and an LBP block for detecting temporally-correlated user activities. Simulation results demonstrate the superiority of the HyVAMP-DCS algorithm.

Acknowledgements
We appreciate the editors and reviewers who processed and reviewed our manuscript to provide the detailed professional comments on the technical contributions, logical structure and content presentation of this paper.

Author contributions
YX performed the data analysis, formal analysis, validation and also wrote the manuscript; WL performed the data analysis and validation.

Funding
Not applicable.

Availability of data and materials
Not applicable.

Declarations

Ethics approval and consent to participate
Not applicable.

Consent for publication
Not applicable.

Competing interests
All authors disclosed no relevant relationships. The authors declared no potential conflicts of interest.

Received: 3 January 2024 Accepted: 9 April 2024
Published online: 16 April 2024

References

1. Y. Wu, S. Tang, L. Zhang, Resilient machine learning based semantic-aware MEC networks for sustainable next-G consumer electronics. IEEE Trans. Consumer Electron. **99**, 1–10 (2023)
2. S. Tang, Q. Yang, L. Fan, Contrastive learning based semantic communications. IEEE Trans. Commun. **99**, 1–12 (2024)
3. X. Chen, D.W.K. Ng, W. Yu, E.G. Larsson, N. Al-Dhahir, R. Schober, Massive access for 5G and beyond. IEEE J. Sel. Areas Commun. **39**(3), 615–637 (2020)
4. C. Bockelmann, N. Pratas, H. Nikopour, K. Au, T. Svensson, C. Stefanovic, P. Popovski, A. Dekorsy, Massive machine-type communications in 5G: physical and MAC-layer solutions. IEEE Commun. Mag. **54**(9), 59–65 (2016)
5. L. Liu, E.G. Larsson, W. Yu, P. Popovski, C. Stefanovic, E. De Carvalho, Sparse signal processing for grant-free massive connectivity: a future paradigm for random access protocols in the Internet of Things. IEEE Signal Process. Mag. **35**(5), 88–99 (2018)
6. L. Liu, W. Yu, Massive connectivity with massive MIMO-part I: device activity detection and channel estimation. IEEE Trans. Signal Process. **66**(11), 2933–2946 (2018)
7. K. Senel, E.G. Larsson, Grant-free massive MTC-enabled massive MIMO: a compressive sensing approach. IEEE Trans. Commun. **66**(12), 6164–6175 (2018)
8. Z. Zhang, Y. Li, C. Huang, Q. Guo, C. Yuen, Y.L. Guan, DNN-aided block sparse Bayesian learning for user activity detection and channel estimation in grant-free non-orthogonal random access. IEEE Trans. Veh. Technol. **68**(12), 12000–12012 (2019)
9. Y. Li, M. Xia, Y.-C. Wu, Activity detection for massive connectivity under frequency offsets via first-order algorithms. IEEE Trans. Wireless Commun. **18**(3), 1988–2002 (2019)
10. H.F. Schepker, C. Bockelmann, A. Dekorsy, Exploiting sparsity in channel and data estimation for sporadic multi-user communication. In: Proc. 10th Int. Symp. Wireless Commun. Syst., pp. 1–5 (2013). VDE
11. Z. Chen, F. Sohrabi, W. Yu, Sparse activity detection for massive connectivity. IEEE Trans. Signal Process. **66**(7), 1890–1904 (2018)
12. Q. Zou, H. Zhang, D. Cai, H. Yang, A low-complexity joint user activity, channel and data estimation for grant-free massive MIMO systems. IEEE Signal Process. Lett. **27**, 1290–1294 (2020)
13. Q. Zou, H. Zhang, D. Cai, H. Yang, Message passing based joint channel and user activity estimation for uplink grant-free massive MIMO systems with low-precision ADCs. IEEE Signal Process. Lett. **27**, 506–510 (2020)

14. S. Liu, H. Zhang, Q. Zou, Decentralized channel estimation for the uplink of grant-free massive machine-type communications. IEEE Trans. Commun. **70**(2), 967–979 (2021)
15. D. Angelosante, G.B. Giannakis, E. Grossi, Compressed sensing of time-varying signals. In: Proc. 16th Int. Conf. Digit. Signal Process., pp. 1–8 (2009). IEEE
16. J. Ziniel, P. Schniter, Dynamic compressive sensing of time-varying signals via approximate message passing. IEEE Trans. Signal Process. **61**(21), 5270–5284 (2013)
17. B. Wang, L. Dai, Y. Zhang, T. Mir, J. Li, Dynamic compressive sensing-based multi-user detection for uplink grant-free NOMA. IEEE Commun. Lett. **20**(11), 2320–2323 (2016)
18. N. Vaswani, W. Lu, Modified-CS: modifying compressive sensing for problems with partially known support. IEEE Trans. Signal Process. **58**(9), 4595–4607 (2010)
19. D. Angelosante, S.I. Roumeliotis, G.B. Giannakis, Lasso-kalman smoother for tracking sparse signals. In: Proc. Asilomar Conf. Signals, Syst., Comput., pp. 181–185 (2009). IEEE
20. J.-C. Jiang, H.-M. Wang, Massive random access with sporadic short packets: Joint active user detection and channel estimation via sequential message passing. IEEE Trans. Wireless Commun. **20**(7), 4541–4555 (2021)
21. Q. Wang, L. Liu, S. Zhang, F.C. Lau, On massive IoT connectivity with temporally-correlated user activity. In: IEEE Int. Symp. on Inf. Theory., pp. 3020–3025 (2021). IEEE
22. J. Pearl, Probabilistic Reasoning in Intelligent Systems: Networks of Plausible Inference, (1988)
23. W. Zhu, M. Tao, X. Yuan, Y. Guan, *Message Passing-Based Joint User Activity Detection and Channel Estimation for Temporally-Correlated Massive Access* (IEEE Trans, Commun, 2023)
24. D.L. Donoho, A. Maleki, A. Montanari, Message-passing algorithms for compressed sensing. Proc. Nat. Acad. Sci. **106**(45), 18914–18919 (2009)
25. Y. Kabashima, A CDMA multiuser detection algorithm on the basis of belief propagation. J. Phys. A: Math. Gen. **36**(43), 11111 (2003)
26. S. Rangan, Generalized approximate message passing for estimation with random linear mixing. In: Proc. IEEE Int. Symp. Inf. Theory., pp. 2168–2172 (2011). IEEE
27. S. Rangan, P. Schniter, A.K. Fletcher, Vector approximate message passing. IEEE Trans. Inf. Theory **65**(10), 6664–6684 (2019)
28. H. He, C.-K. Wen, S. Jin, Generalized expectation consistent signal recovery for nonlinear measurements. In: IEEE Int. Symp. on Inf. Theory., pp. 2333–2337 (2017). IEEE
29. Y. Cheng, L. Liu, L. Ping, Orthogonal AMP for massive access in channels with spatial and temporal correlations. IEEE J. Sel. Areas Commun. **39**(3), 726–740 (2020)
30. T.P. Minka, Expectation propagation for approximate Bayesian inference. arXiv preprint arXiv:1301.2294 (2013)
31. M. Opper, O. Winther, M.J. Jordan, Expectation consistent approximate inference. J. Mach. Learn. Res. **6**(12) (2005)
32. K. Murphy, Y. Weiss, M.I. Jordan, Loopy belief propagation for approximate inference: An empirical study. arXiv preprint arXiv:1301.6725 (2013)
33. P. Schniter, S. Rangan, A.K. Fletcher, Vector approximate message passing for the generalized linear model. In: Proc. Asilomar Conf. Signals, Syst., Comput., pp. 1525–1529 (2016). IEEE

Publisher's Note